

# MeV to multi-TeV thermal WIMPs: most conservative limits

Koushik Dutta,<sup>a</sup> Avirup Ghosh,<sup>b</sup> Arpan Kar,<sup>c,d</sup> Biswarup Mukhopadhyaya<sup>a</sup>

<sup>a</sup>Department of Physical Sciences, Indian Institute of Science Education and Research, Kolkata, Mohanpur - 741246, India.

<sup>b</sup>School of Physical Sciences, Indian Association for the Cultivation of Science, 2A and 2B Raja S.C. Mullick Road, Kolkata 700 032.

<sup>c</sup>Center for Quantum Spacetime, Sogang University, Seoul 121-742, South Korea.

<sup>d</sup>Department of Physics, Sogang University, Seoul 121-742, South Korea.

E-mail: [koushik@iiserkol.ac.in](mailto:koushik@iiserkol.ac.in), [avirup.ghosh1993@gmail.com](mailto:avirup.ghosh1993@gmail.com),  
[arpankarphys@gmail.com](mailto:arpankarphys@gmail.com), [biswarup@iiserkol.ac.in](mailto:biswarup@iiserkol.ac.in)

**Abstract.** We consider a weakly interacting massive particle (WIMP) dark matter (DM) annihilating into all possible Standard Model (SM) particle pairs, including the SM neutrinos, via  $s$ -wave processes and derive the branching ratio independent upper limit on the total annihilation cross-section  $\langle\sigma v\rangle$  using the data of CMB, gamma-ray, cosmic-ray and several neutrino observations. For conservative choices of all relevant astrophysical parameters, we obtain upper limits of  $10^{-23} - 10^{-25} \text{ cm}^3\text{s}^{-1}$  on the total  $\langle\sigma v\rangle$  for the WIMP mass range 10 MeV – 100 TeV, thus making the entire mass range consistent with the observed relic density. An important input that goes into our analysis is the assumption that thermal WIMPs can have significant coupling to the SM neutrinos.

**Keywords:** WIMPs, Planck CMB, Fermi-LAT dSph, AMS-02, H.E.S.S GC, Super-Kamiokande, IceCube, ANTARES

---

## Contents

<b>1</b>	<b>Introduction</b>	<b>2</b>
<b>2</b>	<b>Limits from CMB, <math>\gamma</math>-ray and cosmic-ray observations</b>	<b>3</b>
2.1	Planck	3
2.2	Fermi-LAT	4
2.3	AMS-02	6
2.4	H.E.S.S	8
<b>3</b>	<b>Limits from neutrino observations</b>	<b>9</b>
3.1	Super-Kamiokande	9
3.2	IceCube	11
3.3	ANTARES	11
<b>4</b>	<b>Constraints on total annihilation cross-section</b>	<b>12</b>
<b>5</b>	<b>Conclusions</b>	<b>14</b>
	<b>References</b>	<b>15</b>

---

## 1 Introduction

Weakly interacting massive particles (WIMPs) are widely studied DM candidates of our Universe. A WIMP maintains thermal equilibrium with the Standard Model (SM) plasma in the Early Universe and freezes-out when its annihilation rate falls below the expansion rate of the Universe [1]. The relic density requirement,  $\Omega_\chi h^2 = 0.12$  [1, 2], specifies its thermally averaged total annihilation cross-section,  $\langle\sigma v\rangle \sim 10^{-26} \text{ cm}^3 \text{ s}^{-1}$ , at the time of freeze-out, but does not fix the branching ratio (BR) of each individual annihilation channel. The observed structure of the Universe puts a lower bound of  $\mathcal{O}(\text{keV})$  on the mass ( $m_\chi$ ) of a thermal DM [3], while, the upper bound comes from the unitarity of the S-matrix which disallows  $m_\chi \gtrsim \mathcal{O}(100 \text{ TeV})$  [4, 5]. Therefore, any value of  $m_\chi$  lying in the range MeV - 100 TeV is *prima facie* allowed unless it is ruled out by some existing observations.

Although direct detection experiments [6–12] and collider searches [13–17] have put limits on thermal WIMPs, assumptions on their interactions enter into the derivations of such constraints (see, for example, [18, 19]). Similarly, while analyzing potential WIMP signals in indirect searches, too, assumptions on their annihilation branching fractions are implicit [2, 18–26]. It is on the basis of such assumptions, a WIMP of mass up to *a few hundreds of GeV* is claimed to be ruled out [21–23], since its maximum allowed  $\langle\sigma v\rangle$  falls below  $10^{-26} \text{ cm}^3 \text{ s}^{-1}$ , the value required from relic density.

Note that, such channel specific constraints are not universally applicable. This is because, in a given DM model, DM particles can annihilate into multiple channels with BRs dictated by the model parameters, and in such cases the resulting upper limits on total  $\langle\sigma v\rangle$  can be quite different. However, due to the existence of a large number of DM models it is impossible to perform a study on a model-by-model basis and hence, the most general approach to meaningfully interpret the impact of the observational data on WIMP DM annihilations is to vary the branching ratios of each channel arbitrarily. Following this approach, Ref. [27] claimed that thermal WIMPs annihilating into visible SM final states via  $2 \rightarrow 2$  *s*-wave processes were disallowed for  $m_\chi \lesssim 20 \text{ GeV}$  by the data available till then. On the other hand, while Big-Bang Nucleosynthesis (BBN) and Cosmic Microwave Background (CMB) data rule out  $m_\chi \lesssim 10 \text{ MeV}$  [28, 29] (Ref. [30] suggests stronger BBN constraints under specific assumptions),  $m_\chi$  values much smaller than 20 GeV are in principle permitted if the DM  $\chi$  annihilates substantially into SM neutrinos [25, 31, 32].

In this work, we re-examine the above claim in the most general approach, by considering the possibility of WIMP DM annihilations into SM neutrinos, and only assuming that the dominant annihilations proceed via two-body SM final states. Our conclusion is that the entire  $m_\chi$  range 10 MeV - 100 TeV can be allowed for such WIMP candidates. This conclusion is arrived at, after taking into account the most updated constraints from the relevant neutrino observations [33–39] as well as the CMB [2, 20],  $\gamma$ -ray [21, 40] and cosmic-ray [41] data. Note that, while we are not tilting towards any particular DM model, it turns out that WIMPs of  $m_\chi \lesssim \mathcal{O}(10 \text{ GeV})$  are allowed if they have substantial branching ratios into SM neutrinos. Although such a feature is not very common, it is phenomenologically viable. There exist scenarios where DM lighter than  $\sim 10 \text{ GeV}$  dominantly annihilates into SM neutrinos [42–46] and such models also fall under the purview of the present study. On the whole, the present study has the following novel features:

- The possibility of DM annihilating into  $\nu\bar{\nu}$  pairs has been included in an unbiased manner. This affects our analysis in three ways. First, it allows arbitrary reduction in the branching ratios into *all SM particle pairs other than neutrinos*. Secondly, the

updated constraints ensuing from all neutrino observation experiments [33–36] have been included, especially for cases where the neutrino-pair channel has appreciable branching ratio. And thirdly, for high-mass DM, the energetic neutrinos may have enhanced W-emission rates, resulting in additional contributions to high-energy  $\gamma$ -ray and cosmic-ray events, whose effects on the current constraints have been calculated.

- The most updated data from Planck [2], Fermi-LAT [21] and AMS-02 [41] have been used, once more without any *a priori* assumption regarding the values of the DM annihilation branching ratios.
- The H.E.S.S. data [40] and their relevance for multi-TeV WIMP annihilations have been taken into account.

This paper is organized as follows: in Sec. 2 we describe the limits obtained from CMB,  $\gamma$ -ray and cosmic-ray data. Sec. 3 is devoted to the discussion of the limits coming from the neutrino observations. In Sec. 4 we present the constraints we have obtained on the total annihilation cross-section using all observational data. Finally, we conclude in Sec. 5.

## 2 Limits from CMB, $\gamma$ -ray and cosmic-ray observations

Fluxes of  $\gamma$ ,  $e^-(e^+)$ ,  $\nu(\bar{\nu})$  produced from the cascade decays of the DM annihilation induced SM particle pairs,  $\text{SM}_1\overline{\text{SM}}_2$  (i.e.,  $e^+e^-$ ,  $\mu^+\mu^-$ ,  $\tau^+\tau^-$ ,  $b\bar{b}$ ,  $t\bar{t}$ ,  $q\bar{q}$ ,  $gg$ ,  $W^+W^-$ ,  $ZZ$ ,  $\gamma\gamma$ ,  $hh$ ,  $h\gamma$ ,  $Z\gamma$ ,  $Zh$  and  $\nu\bar{\nu}$ )<sup>1</sup>, are proportional to the total  $\langle\sigma v\rangle$ , for a fixed  $m_\chi$  and a given set of relevant astrophysical parameters. These fluxes are compared with the observed data to derive limits on the  $\langle\sigma v\rangle$ – $m_\chi$  plane. Here, such fluxes are obtained using `Pythia` [47, 48], with the only exceptions being sub-GeV DM annihilations, for which we use the available analytic formulae [49, 50]. Instead of `Pythia` one can use other monte-carlo event generators [51–53] to obtain the DM induced fluxes of stable SM particles. Such fluxes can be sensitive to the choice of the event generator [54–56], and depending on the event generator used, the DM induced  $e^-(e^+)$  and  $\nu(\bar{\nu})$  fluxes may vary up to  $\sim 20\%$ , while the gamma-ray fluxes may change by a factor of a few. Such differences are attributed to the QED and electroweak corrections incorporated in `Pythia`. For annihilation channels leading to hadronic end products like antiprotons, the differences can be even larger and are caused by the differences in the hadronization modelling used by different generators. In this work, we have not considered such dependencies of the DM annihilation fluxes on the event generators and assumed that these fluxes are faithfully simulated using `Pythia`.

Throughout the paper, we shall consider a self-conjugate WIMP DM candidate (e.g., real scalar or Majorana fermion), for illustration. However, it is straightforward to extend our analysis to other possible WIMP scenarios. In this section, we discuss the constraints obtained from the non-observation of DM induced  $\gamma$  and  $e^-(e^+)$  fluxes.

### 2.1 Planck

Ionizing particles (mainly  $e^-$ ,  $e^+$  and  $\gamma$ ) originating from DM annihilations, can change the ionization history of the hydrogen and helium gasses, thereby perturbing CMB anisotropies. Planck [2, 20] measurement of the CMB anisotropy is used to derive the 95% confidence level

---

<sup>1</sup>For  $\nu\bar{\nu}$  final state,  $\nu_e\bar{\nu}_e$ ,  $\nu_\mu\bar{\nu}_\mu$  and  $\nu_\tau\bar{\nu}_\tau$ , while, for  $q\bar{q}$  channel,  $u\bar{u}$ ,  $d\bar{d}$ ,  $c\bar{c}$  and  $s\bar{s}$  are assumed to have equal BRs, so that their sums represent the total branching fractions attributed to  $\nu\bar{\nu}$  and  $q\bar{q}$ , respectively.

(C.L.) upper limit on  $\langle\sigma v\rangle$  for any given DM mass, following the methodology of [57]. As shown in [57], the CMB constraints on the  $\langle\sigma v\rangle - m_\chi$  plane of an annihilating WIMP DM is given by,

$$\epsilon_{\text{eff}}(m_\chi) \frac{\langle\sigma v\rangle}{m_\chi} \lesssim 4.1 \times 10^{-28} \text{ cm}^3 \text{ s}^{-1} \text{ GeV}^{-1}, \quad (2.1)$$

where the weighted efficiency factor,

$$\epsilon_{\text{eff}}(m_\chi) = \frac{1}{2m_\chi} \int_0^{m_\chi} \sum_{f \in \text{SM}_1 \text{SM}_2} \left( 2\epsilon_{e^\pm} B_f \frac{dN_f}{dE_{e^\pm}} E_{e^\pm} dE_{e^\pm} + \epsilon_\gamma B_f \frac{dN_f}{dE_\gamma} E_\gamma dE_\gamma \right). \quad (2.2)$$

Here,  $f$  represents a particular SM final state with branching ratio  $B_f$  and the corresponding electron (photon) spectra are  $dN_f/dE_{e^\pm}$  ( $dN_f/dE_\gamma$ ). The efficiency factors for  $e^\pm$  and  $\gamma$ , i.e.,  $\epsilon_{e^\pm}$  and  $\epsilon_\gamma$ , are taken from [57].

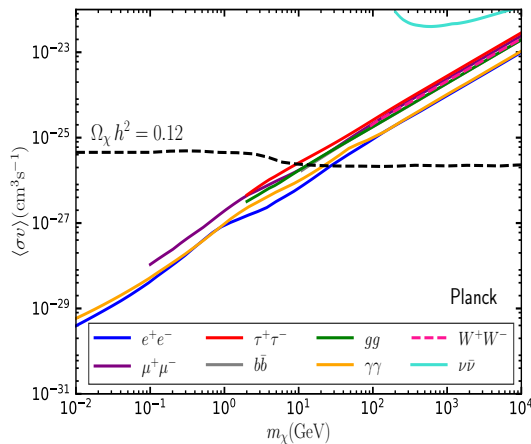


**Figure 1.** The 95% C.L. upper limits on  $\langle\sigma v\rangle$ , obtained from the Planck observation of the CMB anisotropies, are shown for eight representative annihilation channels, assuming 100% BR for each individual final state.

The 95% C.L. upper limits on  $\langle\sigma v\rangle$ , are shown in Fig. 1, for eight representative annihilation channels, assuming 100% BR for each channel. Throughout the considered  $m_\chi$  range, the CMB constraints are strongest for  $\gamma\gamma$  and  $e^+e^-$ , and weakest for  $\nu\bar{\nu}$ . In fact, for  $m_\chi \lesssim 5$  GeV, the strongest constraints for the visible final states (assuming  $s$ -wave annihilations) are obtained from CMB [50]. We note that our limits agree with the limits obtained in [57], since we closely follow the analysis presented there. Moreover, we also checked that the limit for the  $\nu\bar{\nu}$  final state is dominated by  $\nu_e\bar{\nu}_e$ , as shown in [57]. The only uncertainties associated with the CMB limits stem from the  $e^-$  ( $e^+$ ) and the  $\gamma$ -ray spectra of DM annihilations which we have obtained using `Pythia`, and hence the CMB limits are free from all astrophysical uncertainties.

## 2.2 Fermi-LAT

Dwarf spheroidal (dSph) galaxies are suitable targets to search for DM annihilation signals due to their high mass-to-light ratios and low astrophysical backgrounds. Hence, the  $\gamma$ -ray data in the energy range 500 MeV – 500 GeV, obtained from the Fermi-LAT observation of

dSphs [58], give strong constraints on the parameter space of annihilating WIMPs. Fermi-LAT collaboration [21] has performed a likelihood analysis of the six years of Fermi-LAT data observed from the directions of the dSphs and derived the 95% C.L. upper limits on the  $\langle\sigma v\rangle$  of WIMPs. They have provided the likelihood curve for each dSph as a function of the bin-by-bin integrated photon energy fluxes in the energy range 500 MeV – 500 GeV [59]. The integrated photon energy flux (in the energy bin  $[E_{\min}, E_{\max}]$ ) for the  $i$ -th dSph is given by:

$$\Phi_{E_i} = \frac{\langle\sigma v\rangle J_i}{8\pi m_\chi^2} \int_{E_{\min}}^{E_{\max}} \sum_{f \in \text{SM}_1 \overline{\text{SM}}_2} B_f \frac{dN_f}{dE_\gamma} E_\gamma dE_\gamma, \quad (2.3)$$

where  $J_i$  is the J-factor of the  $i$ -th dSph. Following [27, 58], we modify the likelihood curve for each dSph,  $\mathcal{L}_i(\mu|\mathcal{D}_i)$  [59] (where  $\mu$  is the model parameter and  $\mathcal{D}_i$  is the  $\gamma$ -ray data for the  $i$ -th dSph), in the following way:

$$\tilde{\mathcal{L}}_i(\mu, J_i|\mathcal{D}_i) = \mathcal{L}_i(\mu|\mathcal{D}_i) \times \frac{1}{\ln(10) J_i \sqrt{2\pi}\sigma_i} e^{-(\log_{10}(J_i) - \overline{\log_{10}(J_i)})^2 / 2\sigma_i^2}. \quad (2.4)$$

Here,  $J_i$  acts as an additional nuisance parameter, with the values of  $\overline{\log_{10}(J_i)}$  and  $\sigma_i$  obtained from [21]. The total likelihood function is obtained by multiplying the individual likelihoods of 41 dSphs [21], which include both kinematically confirmed and likely galaxies. This resulting function is then extremized (as described in [27]) to obtain the 95% C.L. upper limit on  $\langle\sigma v\rangle$ .

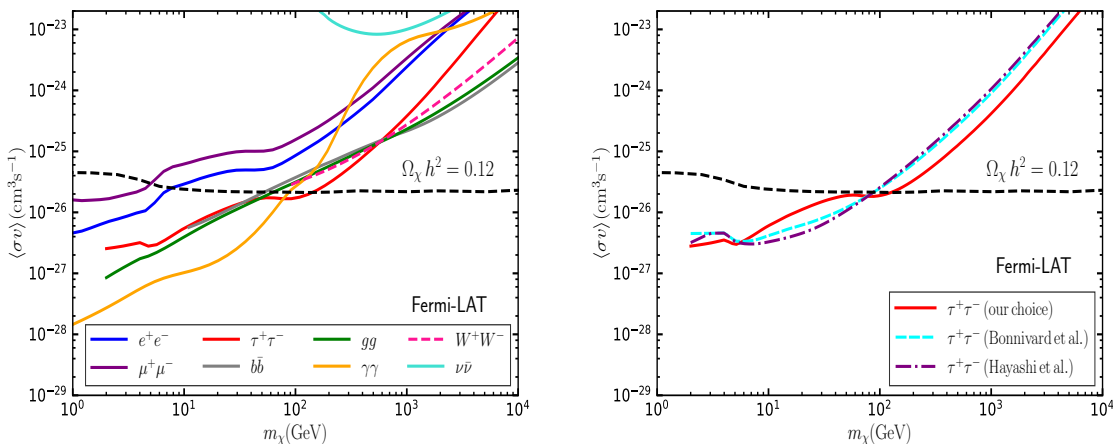


**Figure 2.** *Left:* the 95% C.L. upper limits on  $\langle\sigma v\rangle$ , obtained using the data of the Fermi-LAT dSph gamma-ray observation, are shown. Here, for illustrative purpose, the results for eight annihilation channels (assuming 100% BR) are shown. *Right:* comparison of our limit for the  $\tau^+\tau^-$  channel (red solid) with the limits obtained using the J-factors from [60] (cyan dashed) and [61] (purple dashdotted).

The resulting limits are shown in the left panel of Fig. 2. Here, we have shown the results for eight representative annihilation channels (each with 100% BR). In this case, the  $\gamma\gamma$  channel is most strongly constrained for  $m_\chi \lesssim$  a few hundreds of GeV, while for heavier DMs the constraints on the final states possessing hadronic decay modes (e.g.,  $\tau^+\tau^-$ ,  $b\bar{b}$ ,  $g g$ )

become stronger. Throughout the considered  $m_\chi$  range, the constraints for the  $\nu\bar{\nu}$  channel are the weakest.

Note that the largest uncertainties associated with the Fermi-LAT  $\gamma$ -ray limits come from the measurements of the dSph J-factors. Here, we have considered the J-factors given in [21]. However, there exist several other measurements of the dSph J-factors (e.g., see [60, 61]). The upper limits on  $\langle\sigma v\rangle$  obtained for DM annihilations to  $\tau^+\tau^-$  considering the J-factors reported in [60] (cyan dashed) and [61] (purple dashdotted) are compared against our limit (red solid) in the right panel of Fig. 2. The differences observed in the limits are attributed to the fact that J-factors for all 41 dSphs considered in our analysis are not available in [60, 61] thereby leading to changes in the global likelihood for any given DM mass.

### 2.3 AMS-02

DM annihilations induced positrons undergo diffusion and energy losses while propagating through the Milky Way (MW) halo and can contribute to the AMS-02 observation of the cosmic-ray positron flux in the energy range 500 MeV – 1 TeV [41]. The propagation equation of such positrons is [27],

$$\frac{\partial N_i}{\partial t} = \vec{\nabla} \cdot (D\vec{\nabla})N_i + \frac{\partial}{\partial p}(b(p, \vec{r}))N_i + Q_i(p, \vec{r}) + \sum_{j>i} \beta n_{gas}(\vec{r}) \sigma_{ji} N_j - \beta n_{gas}(\vec{r}) \sigma_i^{\text{in}}(E_k) N_i, \quad (2.5)$$

where the source term for DM annihilations is given by,

$$Q_\chi(p, r, z) = \frac{\rho_\chi^2(r) \langle\sigma v\rangle}{2m_\chi^2} \sum_{f \in \text{SM}_1 \text{SM}_2} B_f \frac{dN_f}{dE_{e^\pm}}. \quad (2.6)$$

In Eq. 2.5, we parameterize the MW diffusion parameter,  $D(\rho, |\vec{r}|, z)$ , as in [27]:

$$D(\rho, |\vec{r}|, z) = D_0 e^{|z|/z_t} \left( \frac{\rho}{\rho_0} \right)^\delta, \quad (2.7)$$

with reference rigidity  $\rho_0 = 4$  GV, diffusion coefficient  $D_0 = 2.7 \times 10^{28} \text{ cm}^2 \text{ s}^{-1}$ , diffusion index  $\delta = 0.6$  and thickness of the axisymmetric diffusion zone  $2z_t = 8$  kpc [27]. The DM induced positron fluxes depend on the values of the diffusion parameters. In order to illustrate how the diffusion parameters may affect the upper limits on  $\langle\sigma v\rangle$ , we shall consider other popular choices of  $D(\rho, |\vec{r}|, z)$  [62, 63].

On the other hand, the energy losses suffered by the positrons during their propagation (governed by the energy loss term  $b(p, \vec{r})$ ), increases with the increase in the value of the galactic magnetic field, thereby weakening the corresponding limits. Therefore, in order to be conservative, we take somewhat larger value of the local magnetic field  $B_\odot = 8.9 \mu\text{G}$  [27]. For a smaller value of  $B_\odot = 5.7 \mu\text{G}$  [23, 64, 65], our limits strengthen by less than a factor of two. The effect of solar modulation is described by the force-field approximation with a modulation potential  $\Phi = 0.6$  GV [66]. On decreasing  $\Phi$  to a value of 0.46 GV [66], the constraints strengthen at most by a factor of two, for  $m_\chi \lesssim 10$  GeV. The dependency of the derived constraints on the value of the solar modulation potential can be alleviated by utilising the  $e^\pm$  data of Voyager 1 in the energy range  $\sim 10 - 50$  MeV [67]. However,

the limits coming from the Voyager 1 data being weaker than the CMB limits (for  $s$ -wave annihilations) [68], our constraints on the total  $\langle\sigma v\rangle$  will remain unaffected with the inclusion of Voyager 1 data.

We assume the DM distribution inside the MW halo,  $\rho_\chi(r)$ , follows the Navarro-Frenk-White (NFW) profile [69]:

$$\rho_\chi(r) = \rho_s \left(\frac{r}{r_s}\right) \left(1 + \frac{r}{r_s}\right)^{-2}, \quad (2.8)$$

with the scale radius  $r_s = 20$  kpc, distance of the Sun from the galactic center (GC)  $r_\odot = 8.5$  kpc and local DM density  $\rho_\odot = 0.25$  GeV cm $^{-3}$  [27]. Such a choice of  $\rho_\odot$  is consistent [70–73] and yields most conservative upper limits on  $\langle\sigma v\rangle$ . On raising  $\rho_\odot$  to 0.7 GeV cm $^{-3}$  [70–73], the limits become stronger by a factor of eight.

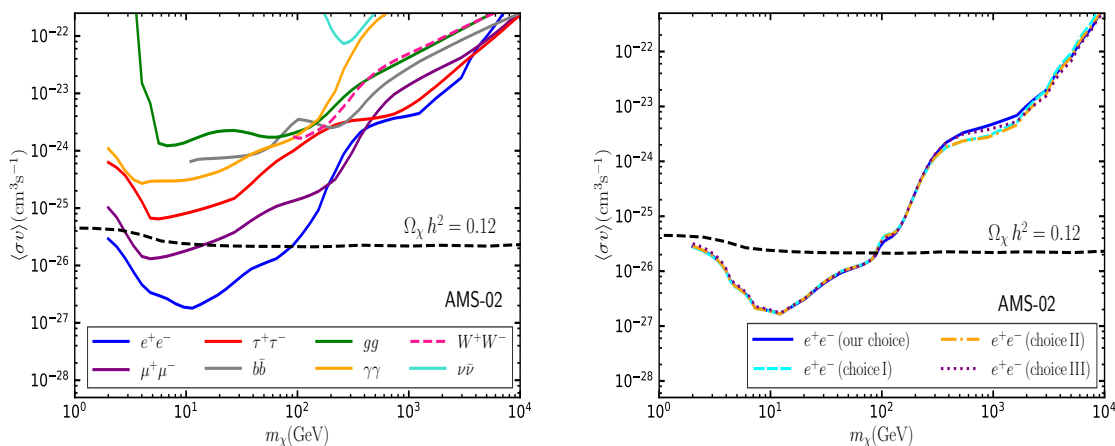


**Figure 3.** *Left:* the 95% C.L. upper limits on  $\langle\sigma v\rangle$ , obtained using AMS-02 cosmic-ray positron flux data, are shown. Here, for the purpose of illustration, the results for eight different annihilation channels (assuming 100% BR) are presented. *Right:* variation of the upper limits on  $\langle\sigma v\rangle$  (for  $e^+e^-$  channel) with the diffusion parameters is presented. Our limit is shown by the blue solid line, while the limits obtained using the diffusion parameter choices of [63] are shown by the cyan dashed, orange dashdotted and purple dotted lines.

Following [27, 74], we parameterize the AMS-02 measured positron flux spectrum as a polynomial function ( $f(\alpha)$ ) of energy and define the  $\chi^2$  as

$$\chi^2 = \sum_{i=\text{bins}} \frac{(f_i(\alpha) - \mathcal{D}_i)^2}{\sigma_i^2}, \quad (2.9)$$

where  $\mathcal{D}_i$  represents the AMS-02 measured positron flux data in the  $i$ -th energy bin and  $\sigma_i$  is the associated uncertainty [41]. This  $\chi^2$  is extremized to obtain the best-fit  $\chi^2$ , i.e.,  $\chi_{\text{bf}}^2$ , which corresponds to the best-fit values of  $\{\alpha\}$ . Then we add the DM induced signal to  $f(\alpha)$  and vary  $\{\alpha\}$  within 30% of their best-fit values. To obtain the AMS-02 constraints on  $\langle\sigma v\rangle$  (at 95% C.L.) for any given  $m_\chi$ , we slowly increase  $\langle\sigma v\rangle$  until  $\chi^2 = \chi_{\text{bf}}^2 + 2.71$ . The resulting limits for eight representative annihilation channels are shown in the left panel of Fig. 3, assuming 100% BR for each channel. Here,  $e^+e^-$  final state is most strongly constrained while  $\nu\bar{\nu}$  is most weakly constrained.

In the right panel of Fig. 3, we have shown the variation of the upper limit on  $\langle\sigma v\rangle$  with the choice of the diffusion parameters assuming 100% BR for  $e^+e^-$  channel. In addition to our choice of  $D(\rho, |\vec{r}|, z)$  (blue solid line), we have also considered three other possibilities, consistent with the current AMS-02 data [63], namely,  $D_0 = 2 \times 10^{28} \text{ cm}^2\text{s}^{-1}$ ,  $\delta = 0.49$ ,  $z_t = 8.4 \text{ kpc}$  (choice I; cyan dashed line),  $D_0 = 1.1 \times 10^{28} \text{ cm}^2\text{s}^{-1}$ ,  $\delta = 0.499$ ,  $z_t = 4.67 \text{ kpc}$  (choice II; orange dashdotted line) and  $D_0 = 5 \times 10^{27} \text{ cm}^2\text{s}^{-1}$ ,  $\delta = 0.509$ ,  $z_t = 2.56 \text{ kpc}$  (choice III; purple dotted line), each with reference rigidity  $\rho_0 = 1 \text{ GV}$ . This clearly demonstrates that our limits are not very sensitive to the choice of the diffusion parameters.

## 2.4 H.E.S.S

H.E.S.S is quite sensitive to very high energy gamma-rays. Thus, for  $m_\chi \gtrsim 200 \text{ GeV}$ , the constraints obtained from the H.E.S.S gamma-ray observation from the Galactic halo [40] are stronger than those coming from other data. We assume that a NFW profile (with  $r_s = 20 \text{ kpc}$ ,  $r_\odot = 8.5 \text{ kpc}$  and  $\rho_\odot = 0.25 \text{ GeV cm}^{-3}$ ) describes the MW DM distribution, and adopt the ON-OFF procedure, as described in [40], to derive the H.E.S.S constraints. The ON and the OFF source regions are two well-separated regions inside the galactic halo, such that, the DM induced signal events coming from the ON region are significantly larger than those coming from the OFF region. Here, ON region is an annular ring centered around the GC with inner radius  $0.5^\circ$  and outer radius  $3^\circ$ , excluding the galactic latitude  $|b| < 0.3^\circ$  region along the galactic plane. This ON region is further subdivided into 25 regions of interests (ROIs), each being an annular ring of width  $0.1^\circ$  [40]. OFF source regions are of the same size as the ON region, but ON and OFF regions are situated symmetrically about the pointing positions of the telescope [40].

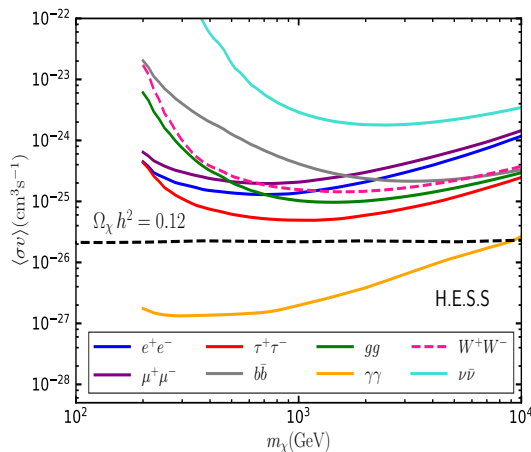


**Figure 4.** For eight representative annihilation channels, the 95% C.L. upper limits on  $\langle\sigma v\rangle$ , obtained from the Galactic halo gamma-ray observation by H.E.S.S, are shown. Here, we have assumed 100% BR for each individual SM final state.

The number of signal events expected from the ON and the OFF regions are given

by [40]:

$$N_{i,\text{ON(OFF)}}^S = \frac{\langle\sigma v\rangle J_{i,\text{ON(OFF)}}}{8\pi m_\chi^2} T_{\text{obs}} \int_{E_{\text{th}}}^{m_\chi} \int_0^\infty dE'_\gamma dE_\gamma \sum_{f \in \text{SM}_1 \overline{\text{SM}}_2} B_f \frac{dN_f}{dE_\gamma}(E_\gamma) A_{\text{eff}}(E_\gamma) R(E_\gamma, E'_\gamma), \quad (2.10)$$

where  $i$  denotes the  $i$ -th ROI and  $J_{i,\text{ON(OFF)}}$  represent the  $J$ -factors for the  $i$ -th ON (OFF) regions. In Eq. 2.10,  $A_{\text{eff}}$  represents the H.E.S.S effective area [75],  $R(E_\gamma, E'_\gamma)$  is a gaussian function accounting for the detector energy resolution of 10% [40] and  $T_{\text{obs}}$  is the H.E.S.S observation time which is 546 hours [40]. Taking the expected number of background events ( $N_i^B$ ) into account, we construct a likelihood function [40],

$$\mathcal{L}_i = \frac{(N_{i,\text{ON}}^S + N_i^B)^{N_{\text{ON},i}}}{N_{\text{ON},i}!} e^{-(N_{i,\text{ON}}^S + N_i^B)} \frac{(N_{i,\text{OFF}}^S + N_i^B)^{N_{\text{OFF},i}}}{N_{\text{OFF},i}!} e^{-(N_{i,\text{OFF}}^S + N_i^B)}, \quad (2.11)$$

where  $N_{\text{ON},i}$  and  $N_{\text{OFF},i}$  represent the respective number of observed  $\gamma$ -ray events from the  $i$ -th ON and OFF regions. The total likelihood function,  $\mathcal{L} = \prod_i \mathcal{L}_i$ , is then extremized following the methodology of [76], to obtain the 95% C.L. upper limits on  $\langle\sigma v\rangle$ .

The resulting limits for eight representative annihilation channels, each with 100% BR, are shown in Fig. 4. In this case,  $\gamma\gamma$  is most strongly constrained while  $\nu\bar{\nu}$  is most weakly constrained. The largest possible uncertainty in this case is associated with the value of the  $\rho_\odot$  and its variation affects these constraints at most by a factor of eight.

Since  $e^-(e^+)$  and  $\gamma$ -ray fluxes from the DM annihilation induced primary  $\nu\bar{\nu}$  pairs are produced via the radiation of electroweak gauge bosons,  $\nu\bar{\nu}$  channel is most weakly constrained, especially for low  $m_\chi$ . Nevertheless,  $W$ -radiations from these neutrinos are important in the context of H.E.S.S observation for  $m_\chi \gtrsim 800$  GeV.

### 3 Limits from neutrino observations

Neutrino telescopes detect the (anti)neutrinos (instead of the  $e^-(e^+)$  and  $\gamma$ -ray photons) coming from DM annihilations, thereby providing strongest constraints for the primary  $\nu\bar{\nu}$  channel. Here, we consider the data of three different neutrino observations, assuming the DM distribution inside the MW halo follows a NFW profile (see Eq. 2.8) with the conservative set of parameters, discussed earlier.

#### 3.1 Super-Kamiokande

**Atmospheric neutrino observation:** The neutrino fluxes measured from the MW halo by the Super-Kamiokande [77] is used to constrain 100 MeV - 10 TeV thermal WIMPs [33, 78]. In obtaining these limits, the ON-OFF analysis method outlined in [33] is adopted, assuming the ON region to be a circle centered around the GC and the OFF region to be another equal-sized circular region offset by  $180^\circ$  in right ascension with respect to the GC [33]. DM annihilation induced neutrino+antineutrino flux distributions from the ON and the OFF source regions are given by:

$$\frac{d\Phi_{\text{ON(OFF)}}}{dE_\nu} = \frac{\langle\sigma v\rangle J_{\text{ON(OFF)}}}{8\pi m_\chi^2} \sum_{f \in \text{SM}_1 \overline{\text{SM}}_2} B_f \left( \frac{dN_f}{dE_\nu} + \frac{dN_f}{dE_{\bar{\nu}}} \right), \quad (3.1)$$

where,  $J_{\text{ON}}$  and  $J_{\text{OFF}}$  represent the  $J$ -factors for the ON and the OFF regions, respectively. While obtaining the neutrino (antineutrino) spectrum  $dN_f/dE_\nu$  ( $dN_{\bar{f}}/dE_{\bar{\nu}}$ ), the effects of neutrino oscillations during propagation has been taken into account, following [33]. Using these flux distributions and the formulae given in [79], we obtain the number of signal events expected from ON and OFF source regions. For the corresponding background events, the distributions of atmospheric neutrinos are obtained from [80]. For  $m_\chi \lesssim 1$  GeV, the fully contained (FC) sub-GeV data sample collected from source regions of half-opening angle  $60^\circ$  [33] is used, while, for  $m_\chi \gtrsim 1$  GeV, the partially contained (PC) and Upward-going through muon (UP- $\mu$ ) events are considered assuming source regions of half-opening angles  $20^\circ$  and  $10^\circ$ , respectively [33].

For each event category, we calculate the asymmetry,  $A = (N_{\text{ON}} - N_{\text{OFF}})/(N_{\text{ON}} + N_{\text{OFF}})$ , with  $N_{\text{ON}}$  and  $N_{\text{OFF}}$  being the total number of signal+background events expected from the ON and the OFF source regions, respectively. This asymmetry parameter is compared with its measured value (provided in [33]) to obtain the upper limit on  $\langle\sigma v\rangle$  for any given  $m_\chi$ . Assuming 100% BR for each channel, one finds that  $\nu\bar{\nu}$  (cyan solid line in Fig. 5) is the most strongly constrained final state, while  $\mu^+\mu^-$  (purple solid line in Fig. 5) is the second most strongly constrained channel. The limits for the remaining annihilation channels are weaker. With the variation of  $\rho_\odot$ , these limits may vary by a factor of eight.

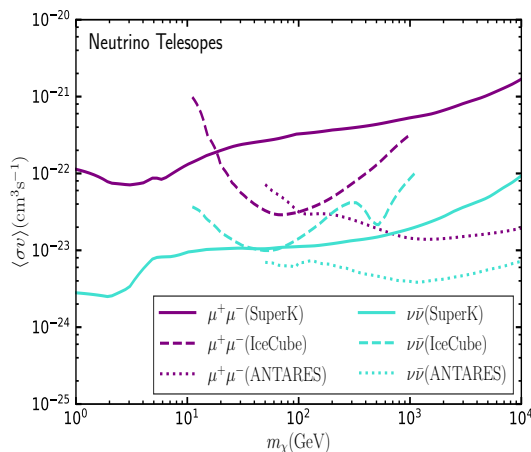


**Figure 5.** 95% C.L. upper limits on  $\langle\sigma v\rangle$  for  $\nu\bar{\nu}$  (cyan) and  $\mu^+\mu^-$  (purple) final states, obtained using the data of Super-Kamiokande (solid lines), IceCube (dashed lines) and ANTARES (dotted lines) telescopes are shown, assuming 100% BR for each channel.

**Diffuse Supernova Neutrino Background (DSNB) observation:** For 10 MeV - 100 MeV WIMPs, the strongest constraint for annihilation into the  $\nu\bar{\nu}$  channel comes from the data of the low-energy neutrino search by the Super-Kamiokande which is commonly used to constrain the diffuse supernova neutrino background (DSNB) [34]. 5823 live time days of all-sky data, ranging from 9 MeV - 88 MeV positron energies [34], have been used (following the methodology of [81, 82]) to derive the 95% C.L. upper limits on  $\langle\sigma v\rangle$ . In this case, the background positron distributions are obtained from [83].

### 3.2 IceCube

Data from 1005 days of neutrino observation of the MW halo by the IceCube is used to constrain 10 GeV - 1 TeV WIMPs [35]. Assuming a source region, extended from 0 to  $2\pi$  radian in right ascension (RA) and -1 to +1 in declination (DEC) [35], the distribution of the DM induced signal events,

$$N_i^S = \frac{\langle\sigma v\rangle J_i}{8\pi m_\chi^2} T_{\text{obs}} \int_0^{m_\chi} \sum_{f \in \text{SM}_1 \overline{\text{SM}}_2} B_f \left( \frac{dN_f}{dE_\nu} A_{\text{eff}}(E_\nu) dE_\nu + \frac{dN_f}{dE_{\bar{\nu}}} A_{\text{eff}}(E_{\bar{\nu}}) dE_{\bar{\nu}} \right), \quad (3.2)$$

is obtained as a function of RA and DEC [35], including the effects of neutrino oscillations [33]. In Eq. 3.2,  $J_i$  represents the  $J$ -factor for the  $i$ -th spatial bin,  $T_{\text{obs}}$  is the IceCube observation time and  $A_{\text{eff}}$  is the IceCube effective area [35]. The distribution in Eq. 3.2 is normalized to obtain the normalized signal event distribution  $f_s$ , while, the normalized background distribution ( $f_B$ ) for the considered observation region is obtained from [35].

These normalized signal and background distributions are combined to form the total event distribution [35, 39],

$$f(\mu) = \mu f_s + (1 - \mu) f_B, \quad (3.3)$$

where  $\mu \in [0, 1]$  represents the fraction of signal events present in the total sample. Thereafter,  $f(\mu)$  is combined with the observed data to construct a likelihood function (as in [35, 39]):

$$\mathcal{L}(\mu) = \prod_i \frac{(n_{\text{obs}}^{\text{tot}} f_i(\mu))^{n_{\text{obs},i}}}{n_{\text{obs},i}!} e^{-n_{\text{obs}}^{\text{tot}} f_i(\mu)}, \quad (3.4)$$

with  $n_{\text{obs}}^{\text{tot}}$  being the total number of observed neutrino events and  $n_{\text{obs},i}$  representing the neutrino events observed in the  $i$ -th spatial bin by the IceCube. This likelihood function is then extremized following the methodology of [84] to derive the 95% C.L. upper limit on  $\mu$ , i.e.,  $\mu_{95\%}$ , for each annihilation channel and a given DM mass. This upper limit is then converted to 95% C.L. upper limit on  $\langle\sigma v\rangle$ . We show the results for  $\nu\bar{\nu}$  (cyan dashed line) and  $\mu^+\mu^-$  (purple dashed line) in Fig. 5, assuming 100% BR for each channel.

### 3.3 ANTARES

Using 2102 days of data of the neutrino observation towards the central region of the MW halo by the ANTARES telescope [37], we constrain WIMPs of masses 50 GeV - 100 TeV. The source region is assumed to be a circle centered around the GC with half-opening angle  $\psi = 30^\circ$  [37] and the normalized angular distribution of the  $\nu_\mu$ -type signal events ( $f_s$ ) is calculated as a function of  $\psi$  (as in the case of IceCube). Here, the detector effective area is taken from [85]. The normalized background event distribution ( $f_B$ ) for the same observation region is obtained from [37]. Then, using the neutrino data observed by ANTARES, predicted signal distribution ( $f_s$ ) and background distribution ( $f_B$ ), we construct a likelihood function as in Eq. 3.4 and follow the methodology of [37, 39] to obtain the 95% C.L. upper limit on the fraction of signal events  $\mu$ , i.e.,  $\mu_{95\%}$ . This is then converted to 95% C.L. upper limit on  $\langle\sigma v\rangle$ , for any given  $m_\chi$ . The resulting constraints for  $\nu\bar{\nu}$  (cyan dotted line) and  $\mu^+\mu^-$  (purple dotted line) channels are presented in Fig. 5.

Note that, for  $m_\chi \gtrsim 800$  GeV, H.E.S.S provides the strongest constraints for  $\nu\bar{\nu}$  (compare Figs. 4 and 5).

## 4 Constraints on total annihilation cross-section

The constraints coming from the data of the indirect search observations depend on the spectrum of photons,  $e^-(e^+)$  and neutrinos produced in DM annihilations. As a result, the BRs of different annihilation channels play important roles in constraining total  $\langle\sigma v\rangle$ . Ref. [27] provides the BR-independent upper limit on the total  $\langle\sigma v\rangle$  of a thermal WIMP without taking into account the possibility of annihilation into  $\nu\bar{\nu}$  channel and the data of the neutrino observations. Although Ref. [57] has pointed out that the CMB limits for the neutrino final states are comparable to the limits coming from the neutrino observations [86–88], a dedicated analysis considering all possible BRs of the  $\nu\bar{\nu}$  channel and using the updated data from the neutrino observations is still lacking. In addition, the inclusion of H.E.S.S data (primarily from the gamma-ray observation of the Galactic halo [40]) also has important implications for annihilation of multi-TeV WIMPs. Here, we consider the possibilities of DM annihilations into all possible SM particle pairs, including  $\nu\bar{\nu}$ , and use the data of all observations (discussed in secs. 2 and 3) to obtain the most general BR-independent upper limit on the total  $\langle\sigma v\rangle$ .

The method for obtaining this BR-independent upper limit on the total  $\langle\sigma v\rangle$  is broadly as follows:

- For each  $m_\chi$ , in the range 10 MeV – 100 TeV, we scan over all possible BR combinations of the kinematically allowed two-body annihilation channels, with grid-size of 2% along any BR axis, ensuring that the BRs of all channels always add up to 100%.
- For each such combination, we derive the 95% C.L. upper limits on  $\langle\sigma v\rangle$  coming from all observations, and find the smallest (i.e., the strongest) limit among these. This limit represents the maximum allowed  $\langle\sigma v\rangle$ , consistent with all observational data, for that particular BR combination.
- Among these allowed values of  $\langle\sigma v\rangle$  obtained for different BR combinations, we find the largest (i.e., the weakest) one, which is the maximum allowed total  $\langle\sigma v\rangle$ , for the considered value of  $m_\chi$ .

For further details of the analysis methodology, see [27, 74]. In obtaining the limits on  $\langle\sigma v\rangle$ , we assume a single-component WIMP accounts for the entire DM content.

Considering DM annihilations to visible SM channels, the 95% C.L. upper limit on total  $\langle\sigma v\rangle$ , allowed by all existing data (green solid line in Fig. 6), is obtained. Here, decisive roles are played by the CMB data for  $m_\chi \lesssim 5$  GeV, Fermi-LAT and AMS-02 data for  $5$  GeV  $\lesssim m_\chi \lesssim 200$  GeV, and H.E.S.S data for  $m_\chi \gtrsim 200$  GeV. The black dashed line represents the thermal relic cross-section for a single-component WIMP, which is larger than the maximum allowed  $\langle\sigma v\rangle$  for  $m_\chi \lesssim 18$  GeV. Thermal WIMPs annihilating into visible SM channels, are thus, ruled out up to  $m_\chi \sim 18$  GeV. Unitarity upper bound on the total  $\langle\sigma v\rangle$  is shown by the purple line [4, 5]. Comparison of our limit with that of [27] (green dashed line in Fig. 6) shows that, inclusion of H.E.S.S data improves the limits on total  $\langle\sigma v\rangle$  for  $m_\chi \gtrsim 200$  GeV, so that a smaller region in the  $\langle\sigma v\rangle - m_\chi$  plane remains allowed.

While considering WIMP annihilations into  $\nu\bar{\nu}$ , we scan over all possible BR combinations (i.e., 0% – 100%) of the kinematically allowed SM channels and obtain the orange line shown in Fig. 7, which represents the maximum allowed total  $\langle\sigma v\rangle$  for a thermal WIMP, retaining the consistency with all existing data. Note that, this limit is dictated by the Super-Kamiokande data of low energy neutrino search for  $m_\chi \lesssim 100$  MeV, Super-Kamiokande, Ice-Cube and ANTARES data of MW halo neutrino observation for  $100$  MeV  $\lesssim m_\chi \lesssim 800$  GeV

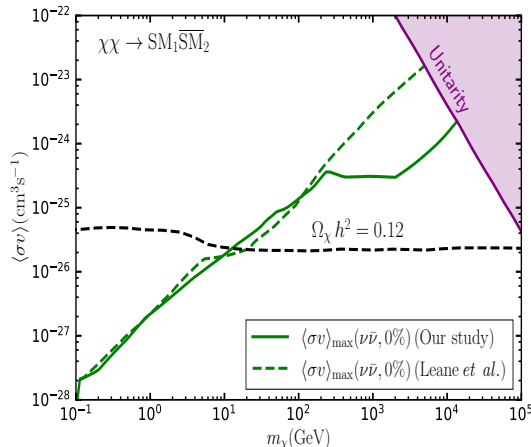


**Figure 6.** For DM annihilations into visible SM final states only, the 95% C.L. upper limit on total  $\langle\sigma v\rangle$  for the  $m_\chi$  range 100 MeV – 100 TeV (green solid line) is shown. Due to the inclusion of H.E.S.S data, our limit is stronger than that of [27] (green dashed line), for  $m_\chi \gtrsim 200$  GeV. The purple line is the unitarity upper bound on total  $\langle\sigma v\rangle$  [4, 5] and the black dashed line represents the cross-section required by a single-component WIMP to achieve  $\Omega_\chi h^2 = 0.12$  [1, 2]. See the text for details.

and H.E.S.S data of the Galactic halo  $\gamma$ -ray observation for  $m_\chi \gtrsim 800$  GeV. For all  $m_\chi$ , this largest allowed  $\langle\sigma v\rangle$  closely follows the upper limit obtained for exactly 100% BR attributed to  $\nu\bar{\nu}$ . This maximum total  $\langle\sigma v\rangle$  comes down for smaller values of  $\nu\bar{\nu}$  BRs (the green lines), but still stays above the black dashed line for significant parts of the parameter space. The gray region is ruled out for all possible BR combinations, and the blue region is disallowed by BBN [28, 29].

We emphasize that, in obtaining these maximum  $\langle\sigma v\rangle$  (orange and green lines) the DM induced fluxes are calculated assuming a single-component WIMP constitutes all the DM in the galaxies. On the other hand, the black dashed curve signifies the minimum  $\langle\sigma v\rangle$  allowed for a single-component DM that does not overclose the Universe. Therefore, the intermediate region below the orange curve and above the black dashed line is *always allowed*. However, for a point lying within this region of the  $\langle\sigma v\rangle - m_\chi$  plane, the relic density is in fact undersaturated by  $\chi$ . The resulting dilution of the annihilating DM flux, moves the maximum allowed  $\langle\sigma v\rangle$  for any  $m_\chi$ , above the orange line. But this does not affect the general conclusion: *a WIMP DM candidate annihilating into two-body SM final states (via s-wave processes), with mass in the range 10 MeV - 100 TeV, can be allowed by all currently available data.*

Note that, this allowed mass range for a thermal WIMP changes with the BR attributed to  $\nu\bar{\nu}$ , as is evident from the green lines shown in Fig. 7. As we decrease the BR into  $\nu\bar{\nu}$ , kinematically allowed visible channels start contributing to the DM induced fluxes, thereby strengthening the upper limit on total  $\langle\sigma v\rangle$ . For example, if one assigns only  $\sim 0.02\%$  BR to visible channels, the constraint on total  $\langle\sigma v\rangle$  becomes stronger (dotted line), but the entire mass range 10 MeV - 100 TeV still remains allowed. If the BR of  $\nu\bar{\nu}$  is decreased further, the upper limit on total  $\langle\sigma v\rangle$  gradually strengthens, until all  $m_\chi$  lower than  $\sim 18$  GeV become ruled out for DM annihilations to only visible SM channels (solid line). Therefore, it is evident that WIMPs of  $m_\chi \lesssim \mathcal{O}(10 \text{ GeV})$  are allowed only if they dominantly annihilate into

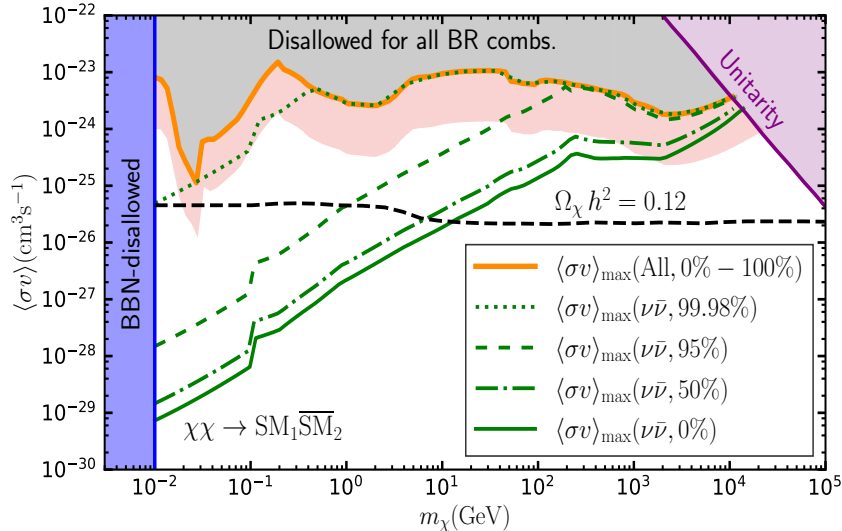


**Figure 7.** For a single-component thermal WIMP in the  $m_\chi$  range 10 MeV - 100 TeV, constituting all the observed DM, the orange line represents the BR-independent upper limit on total  $\langle\sigma v\rangle$  (at 95% C.L.) and the light red band shows its variation with the astrophysical uncertainties. The gray region is ruled out for all possible BR combinations, while, the blue region is disallowed by BBN [28, 29]. The purple and the black dashed lines are the same as in Fig. 6. Variation of the maximum allowed total  $\langle\sigma v\rangle$  with the BR attributed to  $\nu\bar{\nu}$  are shown by the green lines. See the text for details.

SM neutrinos. Such a feature can be realized by invoking extra symmetries and light sterile neutrinos which significantly couple to both the SM neutrinos and the DM [42–46].

It is to be noted that the dependency of our results on the values of the astrophysical parameters is also explored. Since the choice of  $D(\rho, |\vec{r}|, z)$  does not affect the limits considerably (see Fig. 3; right panel), we keep it fixed at  $D_0 = 2.7 \times 10^{28} \text{ cm}^2 \text{ s}^{-1}$ ,  $\delta = 0.6$  and  $z_t = 4 \text{ kpc}$ , but vary  $B_\odot$  in the range  $5.7 - 8.9 \mu\text{G}$  [23, 27],  $\Phi$  within  $0.46 - 0.6 \text{ GV}$  [66] and  $\rho_\odot$  in the range  $0.25 - 0.7 \text{ GeV cm}^{-3}$  [70–73]. On the other hand, we have kept the values of the dSph J-factors fixed at the values given in [21]. The resulting BR-independent upper limits always lie within the light red band (see Fig. 7) which is above the black dashed line for most of the  $m_\chi$  values in the 10 MeV – 100 TeV range. We find that the variation of  $\rho_\odot$  has the most prominent impact on this maximum allowed total  $\langle\sigma v\rangle$ .

## 5 Conclusions

In this work, we have obtained the most conservative BR-independent upper limit on the total  $\langle\sigma v\rangle$  of a 10 MeV - 100 TeV thermal WIMP, annihilating into all possible SM final states via  $2 \rightarrow 2$   $s$ -wave processes, using the most updated data from several astrophysical and cosmological observations, i.e, Planck [2, 20], Fermi-LAT [21], AMS-02 [41], H.E.S.S [40], Super-Kamiokande [33, 34], IceCube [35] and ANTARES [37]. In deriving this constraint, we vary the BRs of all kinematically allowed annihilation channels arbitrarily in the range 0% – 100% and find that the maximum allowed total  $\langle\sigma v\rangle$  lies in the range  $10^{-23} - 10^{-25} \text{ cm}^3 \text{ s}^{-1}$  for the entire  $m_\chi$  range considered. This limit strengthens at most by an order of magnitude with the variations of the astrophysical parameters. We note that, this upper limit on the total

$\langle\sigma v\rangle$  almost always coincides with the upper limit obtained for exactly 100% BR attributed to  $\nu\bar{\nu}$ . As the BR of  $\nu\bar{\nu}$  decreases, the constraint gradually strengthens and for annihilations into visible final states only, thermal WIMPs are ruled out up to  $\sim 18$  GeV. Therefore, for  $m_\chi \lesssim \mathcal{O}(10\text{ GeV})$ , WIMPs are allowed provided they dominantly annihilate into SM neutrinos. In addition, the importance of H.E.S.S data in constraining multi-TeV WIMPs is also emphasized. It is the inclusion of H.E.S.S data which strengthens our limit compared to that obtained in [27], for  $m_\chi \gtrsim 200$  GeV. Several future generation observations [89–112], in particular, the neutrino observations [98–112] and the observations that can constrain  $\rho_\odot$  [113, 114], will improve the constraints on the total  $\langle\sigma v\rangle$  of thermal WIMPs.

Note that, instead of two-body annihilation channels if the WIMP possesses multi-body annihilation channels, including those involving dark sector particles [115–118], the upper-limits on the total  $\langle\sigma v\rangle$  are even weaker [119–121]. Furthermore, for WIMP annihilations dominated by  $p$ -wave processes,  $\langle\sigma v\rangle$  is proportional to the square of the DM relative velocity, whose value in the present day galaxies is suppressed by a few orders of magnitude compared to its value at freeze-out. Hence, in such cases, the relic density constraint becomes less restrictive, in terms of the present value of  $\langle\sigma v\rangle$  [25, 122]<sup>2</sup>. A similar relaxation is expected if co-annihilations contribute to thermal freeze-out. These further strengthen our claim that, in general, thermal WIMPs in the entire 10 MeV - 100 TeV range, are still consistent with all observational data.

## Acknowledgements

The work of K.D. is partially supported by the Indo-Russian grant DST/INT/RUS/RSF/P-21, MTR/2019/000395, and Core Research Grant CRG/2020/004347 funded by SERB, DST, Government of India. The research of A.K. was supported by the National Research Foundation of Korea(NRF) funded by the Ministry of Education through the Center for Quantum Space Time (CQUeST) with grant number 2020R1A6A1A03047877 and by the Ministry of Science and ICT with grant number 2021R1F1A1057119.

## References

- [1] G. Steigman, B. Dasgupta and J. F. Beacom, *Precise Relic WIMP Abundance and its Impact on Searches for Dark Matter Annihilation*, *Phys. Rev. D* **86** (2012) 023506, [1204.3622].
- [2] PLANCK collaboration, N. Aghanim et al., *Planck 2018 results. VI. Cosmological parameters*, *Astron. Astrophys.* **641** (2020) A6, [1807.06209].
- [3] V. Iršič et al., *New Constraints on the free-streaming of warm dark matter from intermediate and small scale Lyman- $\alpha$  forest data*, *Phys. Rev. D* **96** (2017) 023522, [1702.01764].
- [4] K. Griest and M. Kamionkowski, *Unitarity Limits on the Mass and Radius of Dark Matter Particles*, *Phys. Rev. Lett.* **64** (1990) 615.
- [5] J. Smirnov and J. F. Beacom, *TeV-Scale Thermal WIMPs: Unitarity and its Consequences*, *Phys. Rev. D* **100** (2019) 043029, [1904.11503].

---

<sup>2</sup>Although the annihilation cross-section of fermionic scalar portal DM is  $p$ -wave suppressed, their scattering cross-section with protons is unsuppressed [123], thereby leading to direct search constraints on the parameter space of such DM candidate [124, 125].

- [6] XENON collaboration, E. Aprile et al., *Dark Matter Search Results from a One Ton-Year Exposure of XENON1T*, *Phys. Rev. Lett.* **121** (2018) 111302, [[1805.12562](#)].
- [7] LUX collaboration, D. S. Akerib et al., *Results from a search for dark matter in the complete LUX exposure*, *Phys. Rev. Lett.* **118** (2017) 021303, [[1608.07648](#)].
- [8] PANDAX-II collaboration, X. Cui et al., *Dark Matter Results From 54-Ton-Day Exposure of PandaX-II Experiment*, *Phys. Rev. Lett.* **119** (2017) 181302, [[1708.06917](#)].
- [9] DARKSIDE collaboration, P. Agnes et al., *Low-Mass Dark Matter Search with the DarkSide-50 Experiment*, *Phys. Rev. Lett.* **121** (2018) 081307, [[1802.06994](#)].
- [10] CRESST COLLABORATION collaboration, A. H. Abdelhameed, G. Angloher, P. Bauer, A. Bento, E. Bertoldo, C. Bucci et al., *First results from the cressst-iii low-mass dark matter program*, *Phys. Rev. D* **100** (Nov, 2019) 102002.
- [11] PICO collaboration, C. Amole et al., *Dark Matter Search Results from the Complete Exposure of the PICO-60 C<sub>3</sub>F<sub>8</sub> Bubble Chamber*, *Phys. Rev. D* **100** (2019) 022001, [[1902.04031](#)].
- [12] M. Schumann, *Direct Detection of WIMP Dark Matter: Concepts and Status*, *J. Phys. G* **46** (2019) 103003, [[1903.03026](#)].
- [13] CMS collaboration, A. M. Sirunyan et al., *Search for dark matter produced with an energetic jet or a hadronically decaying W or Z boson at  $\sqrt{s} = 13$  TeV*, *JHEP* **07** (2017) 014, [[1703.01651](#)].
- [14] <http://cds.cern.ch/record/2205763>.
- [15] <http://cds.cern.ch/record/2632344>.
- [16] CMS collaboration, V. Khachatryan et al., *Searches for invisible decays of the Higgs boson in pp collisions at  $\sqrt{s} = 7, 8,$  and  $13$  TeV*, *JHEP* **02** (2017) 135, [[1610.09218](#)].
- [17] J. Abdallah et al., *Simplified Models for Dark Matter Searches at the LHC*, *Phys. Dark Univ.* **9-10** (2015) 8–23, [[1506.03116](#)].
- [18] G. Arcadi, M. Dutra, P. Ghosh, M. Lindner, Y. Mambrini, M. Pierre et al., *The waning of the WIMP? A review of models, searches, and constraints*, *Eur. Phys. J. C* **78** (2018) 203, [[1703.07364](#)].
- [19] GAMBIT collaboration, P. Athron et al., *Thermal WIMPs and the scale of new physics: global fits of Dirac dark matter effective field theories*, *Eur. Phys. J. C* **81** (2021) 992, [[2106.02056](#)].
- [20] PLANCK collaboration, P. A. R. Ade et al., *Planck 2015 results. XIII. Cosmological parameters*, *Astron. Astrophys.* **594** (2016) A13, [[1502.01589](#)].
- [21] FERMI-LAT, DES collaboration, A. Albert et al., *Searching for Dark Matter Annihilation in Recently Discovered Milky Way Satellites with Fermi-LAT*, *Astrophys. J.* **834** (2017) 110, [[1611.03184](#)].
- [22] B.-Q. Lu and H.-S. Zong, *Limits on dark matter from AMS-02 antiproton and positron fraction data*, *Phys. Rev. D* **93** (2016) 103517, [[1510.04032](#)].
- [23] I. John and T. Linden, *Cosmic-ray positrons strongly constrain leptophilic dark matter*, *JCAP* **12** (2021) 007, [[2107.10261](#)].
- [24] S. Profumo, F. S. Queiroz and C. E. Yaguna, *Extending Fermi-LAT and H.E.S.S. Limits on Gamma-ray Lines from Dark Matter Annihilation*, *Mon. Not. Roy. Astron. Soc.* **461** (2016) 3976–3981, [[1602.08501](#)].
- [25] C. A. Argüelles, A. Diaz, A. Kheirandish, A. Olivares-Del-Campo, I. Safa and A. C. Vincent, *Dark matter annihilation to neutrinos*, *Rev. Mod. Phys.* **93** (2021) 035007, [[1912.09486](#)].

- [26] A. E. Egorov, *Updated constraints on WIMP dark matter by radio observations of M31 – other annihilation channels*, [2208.14186](#).
- [27] R. K. Leane, T. R. Slatyer, J. F. Beacom and K. C. Y. Ng, *GeV-scale thermal WIMPs: Not even slightly ruled out*, *Phys. Rev. D* **98** (2018) 023016, [[1805.10305](#)].
- [28] K. M. Nollett and G. Steigman, *BBN And The CMB Constrain Light, Electromagnetically Coupled WIMPs*, *Phys. Rev. D* **89** (2014) 083508, [[1312.5725](#)].
- [29] K. M. Nollett and G. Steigman, *BBN And The CMB Constrain Neutrino Coupled Light WIMPs*, *Phys. Rev. D* **91** (2015) 083505, [[1411.6005](#)].
- [30] M. Kawasaki, K. Kohri, T. Moroi and Y. Takaesu, *Revisiting Big-Bang Nucleosynthesis Constraints on Dark-Matter Annihilation*, *Phys. Lett. B* **751** (2015) 246–250, [[1509.03665](#)].
- [31] J. F. Beacom, N. F. Bell and G. D. Mack, *General Upper Bound on the Dark Matter Total Annihilation Cross Section*, *Phys. Rev. Lett.* **99** (2007) 231301, [[astro-ph/0608090](#)].
- [32] H. Yuksel, S. Horiuchi, J. F. Beacom and S. Ando, *Neutrino Constraints on the Dark Matter Total Annihilation Cross Section*, *Phys. Rev. D* **76** (2007) 123506, [[0707.0196](#)].
- [33] SUPER-KAMIOKANDE collaboration, K. Abe et al., *Indirect search for dark matter from the Galactic Center and halo with the Super-Kamiokande detector*, *Phys. Rev. D* **102** (2020) 072002, [[2005.05109](#)].
- [34] SUPER-KAMIOKANDE collaboration, K. Abe et al., *Diffuse supernova neutrino background search at Super-Kamiokande*, *Phys. Rev. D* **104** (2021) 122002, [[2109.11174](#)].
- [35] ICECUBE collaboration, M. G. Aartsen et al., *Search for Neutrinos from Dark Matter Self-Annihilations in the center of the Milky Way with 3 years of IceCube/DeepCore*, *Eur. Phys. J. C* **77** (2017) 627, [[1705.08103](#)].
- [36] ANTARES collaboration, A. Albert et al., *Search for dark matter towards the Galactic Centre with 11 years of ANTARES data*, *Phys. Lett. B* **805** (2020) 135439, [[1912.05296](#)].
- [37] A. Albert et al., *Results from the search for dark matter in the Milky Way with 9 years of data of the ANTARES neutrino telescope*, *Phys. Lett. B* **769** (2017) 249–254, [[1612.04595](#)].
- [38] ICECUBE, ANTARES collaboration, N. Iovine, J. A. Aguilar Sánchez, S. Baur, S. R. Gozzini and J. de Dios Zornoza Gómez, *Combined Search for Neutrinos from Dark Matter Annihilation in the Galactic Centre using ANTARES and IceCube*, *PoS ICRC2019* (2021) 522, [[1908.07300](#)].
- [39] ANTARES, ICECUBE collaboration, A. Albert et al., *Combined search for neutrinos from dark matter self-annihilation in the Galactic Center with ANTARES and IceCube*, *Phys. Rev. D* **102** (2020) 082002, [[2003.06614](#)].
- [40] H.E.S.S. collaboration, H. Abdalla et al., *Search for Dark Matter Annihilation Signals in the H.E.S.S. Inner Galaxy Survey*, *Phys. Rev. Lett.* **129** (2022) 111101, [[2207.10471](#)].
- [41] AMS collaboration, M. Aguilar et al., *Towards Understanding the Origin of Cosmic-Ray Positrons*, *Phys. Rev. Lett.* **122** (2019) 041102.
- [42] M. Blennow, E. Fernandez-Martinez, A. Olivares-Del Campo, S. Pascoli, S. Rosauero-Alcaraz and A. V. Titov, *Neutrino Portals to Dark Matter*, *Eur. Phys. J. C* **79** (2019) 555, [[1903.00006](#)].
- [43] P. Ballett, M. Hostert and S. Pascoli, *Dark Neutrinos and a Three Portal Connection to the Standard Model*, *Phys. Rev. D* **101** (2020) 115025, [[1903.07589](#)].
- [44] B. Dutta, S. Ghosh and J. Kumar, *A sub-GeV dark matter model*, *Phys. Rev. D* **100** (2019) 075028, [[1905.02692](#)].
- [45] C. El Aisati, C. Garcia-Cely, T. Hambye and L. Vanderheyden, *Prospects for discovering a neutrino line induced by dark matter annihilation*, *JCAP* **10** (2017) 021, [[1706.06600](#)].

- [46] Y. Farzan, *Flavoring Monochromatic Neutrino Flux from Dark Matter Annihilation*, *JHEP* **02** (2012) 091, [[1111.1063](#)].
- [47] T. Sjöstrand, S. Ask, J. R. Christiansen, R. Corke, N. Desai, P. Ilten et al., *An introduction to PYTHIA 8.2*, *Comput. Phys. Commun.* **191** (2015) 159–177, [[1410.3012](#)].
- [48] J. R. Christiansen and T. Sjöstrand, *Weak Gauge Boson Radiation in Parton Showers*, *JHEP* **04** (2014) 115, [[1401.5238](#)].
- [49] A. Coogan, L. Morrison and S. Profumo, *Hazma: A Python Toolkit for Studying Indirect Detection of Sub-GeV Dark Matter*, *JCAP* **01** (2020) 056, [[1907.11846](#)].
- [50] M. Cirelli, N. Fornengo, B. J. Kavanagh and E. Pinetti, *Integral X-ray constraints on sub-GeV Dark Matter*, *Phys. Rev. D* **103** (2021) 063022, [[2007.11493](#)].
- [51] J. Bellm et al., *Herwig 7.0/Herwig++ 3.0 release note*, *Eur. Phys. J. C* **76** (2016) 196, [[1512.01178](#)].
- [52] J. Bellm et al., *Herwig 7.1 Release Note*, [1705.06919](#).
- [53] SHERPA collaboration, E. Bothmann et al., *Event Generation with Sherpa 2.2*, *SciPost Phys.* **7** (2019) 034, [[1905.09127](#)].
- [54] J. A. R. Cembranos, A. de la Cruz-Dombriz, V. Gammaldi, R. A. Lineros and A. L. Maroto, *Reliability of Monte Carlo event generators for gamma ray dark matter searches*, *JHEP* **09** (2013) 077, [[1305.2124](#)].
- [55] M. Cirelli, G. Corcella, A. Hektor, G. Hutsi, M. Kadastik, P. Panci et al., *PPPC 4 DM ID: A Poor Particle Physicist Cookbook for Dark Matter Indirect Detection*, *JCAP* **03** (2011) 051, [[1012.4515](#)].
- [56] C. Niblaeus, J. M. Cornell and J. Edsjö, *Effect of polarisation and choice of event generator on spectra from dark matter annihilations*, *JCAP* **10** (2019) 079, [[1907.02488](#)].
- [57] T. R. Slatyer, *Indirect dark matter signatures in the cosmic dark ages. I. Generalizing the bound on s-wave dark matter annihilation from Planck results*, *Phys. Rev. D* **93** (2016) 023527, [[1506.03811](#)].
- [58] FERMI-LAT collaboration, M. Ackermann et al., *Searching for Dark Matter Annihilation from Milky Way Dwarf Spheroidal Galaxies with Six Years of Fermi Large Area Telescope Data*, *Phys. Rev. Lett.* **115** (2015) 231301, [[1503.02641](#)].
- [59] [http://www-glast.stanford.edu/pub\\_data/1203/](http://www-glast.stanford.edu/pub_data/1203/).
- [60] V. Bonnivard et al., *Dark matter annihilation and decay in dwarf spheroidal galaxies: The classical and ultrafaint dSphs*, *Mon. Not. Roy. Astron. Soc.* **453** (2015) 849–867, [[1504.02048](#)].
- [61] K. Hayashi, K. Ichikawa, S. Matsumoto, M. Ibe, M. N. Ishigaki and H. Sugai, *Dark matter annihilation and decay from non-spherical dark halos in galactic dwarf satellites*, *Mon. Not. Roy. Astron. Soc.* **461** (2016) 2914–2928, [[1603.08046](#)].
- [62] Y. Génolini et al., *Cosmic-ray transport from AMS-02 boron to carbon ratio data: Benchmark models and interpretation*, *Phys. Rev. D* **99** (2019) 123028, [[1904.08917](#)].
- [63] Y. Génolini, M. Boudaud, M. Cirelli, L. Derome, J. Lavalle, D. Maurin et al., *New minimal, median, and maximal propagation models for dark matter searches with Galactic cosmic rays*, *Phys. Rev. D* **104** (2021) 083005, [[2103.04108](#)].
- [64] R. Beck, *Galactic and Extragalactic Magnetic Fields*, *AIP Conf. Proc.* **1085** (2009) 83–96, [[0810.2923](#)].
- [65] R. Beck and R. Wielebinski, *Magnetic fields in galaxies*, in *Space Sciences Series of ISSI*, pp. 215–230. Springer New York, 2011. DOI.

- [66] I. Cholis, D. Hooper and T. Linden, *A Predictive Analytic Model for the Solar Modulation of Cosmic Rays*, *Phys. Rev. D* **93** (2016) 043016, [[1511.01507](#)].
- [67] E. C. Stone, A. C. Cummings, F. B. McDonald, B. C. Heikkila, N. K. Lal and W. R. Webber, *Voyager 1 observes low-energy galactic cosmic rays in a region depleted of heliospheric ions*, *Science* **341** (2013) 150 – 153.
- [68] M. Boudaud, J. Lavalle and P. Salati, *Novel cosmic-ray electron and positron constraints on MeV dark matter particles*, *Phys. Rev. Lett.* **119** (2017) 021103, [[1612.07698](#)].
- [69] J. F. Navarro, C. S. Frenk and S. D. M. White, *The Structure of cold dark matter halos*, *Astrophys. J.* **462** (1996) 563–575, [[astro-ph/9508025](#)].
- [70] P. Salucci, F. Nesti, G. Gentile and C. F. Martins, *The dark matter density at the Sun’s location*, *Astron. Astrophys.* **523** (2010) A83, [[1003.3101](#)].
- [71] J. Bovy and S. Tremaine, *On the local dark matter density*, *Astrophys. J.* **756** (2012) 89, [[1205.4033](#)].
- [72] M. Benito, A. Cuoco and F. Iocco, *Handling the Uncertainties in the Galactic Dark Matter Distribution for Particle Dark Matter Searches*, *JCAP* **03** (2019) 033, [[1901.02460](#)].
- [73] M. Benito, F. Iocco and A. Cuoco, *Uncertainties in the Galactic Dark Matter distribution: An update*, *Phys. Dark Univ.* **32** (2021) 100826, [[2009.13523](#)].
- [74] K. Dutta, A. Ghosh, A. Kar and B. Mukhopadhyaya, *A general study of decaying scalar dark matter: existing limits and projected radio signals at the SKA*, *JCAP* **09** (2022) 005, [[2204.06024](#)].
- [75] J. Veh, *Dark matter  $\gamma$ -line search in the galactic centre with h.e.s.s. using an on-off technique*, 2018.
- [76] G. Cowan, K. Cranmer, E. Gross and O. Vitells, *Asymptotic formulae for likelihood-based tests of new physics*, *Eur. Phys. J. C* **71** (2011) 1554, [[1007.1727](#)].
- [77] SUPER-KAMIOKANDE collaboration, E. Richard et al., *Measurements of the atmospheric neutrino flux by Super-Kamiokande: energy spectra, geomagnetic effects, and solar modulation*, *Phys. Rev. D* **94** (2016) 052001, [[1510.08127](#)].
- [78] R. Primulando and P. Uttayarat, *Dark Matter-Neutrino Interaction in Light of Collider and Neutrino Telescope Data*, *JHEP* **06** (2018) 026, [[1710.08567](#)].
- [79] L. Covi, M. Grefe, A. Ibarra and D. Tran, *Neutrino Signals from Dark Matter Decay*, *JCAP* **04** (2010) 017, [[0912.3521](#)].
- [80] M. Honda, T. Kajita, K. Kasahara and S. Midorikawa, *Improvement of low energy atmospheric neutrino flux calculation using the JAM nuclear interaction model*, *Phys. Rev. D* **83** (2011) 123001, [[1102.2688](#)].
- [81] A. Olivares-Del Campo, C. Bohm, S. Palomares-Ruiz and S. Pascoli, *Dark matter-neutrino interactions through the lens of their cosmological implications*, *Phys. Rev. D* **97** (Apr, 2018) 075039.
- [82] S. Palomares-Ruiz and S. Pascoli, *Testing MeV dark matter with neutrino detectors*, *Phys. Rev. D* **77** (2008) 025025, [[0710.5420](#)].
- [83] SUPER-KAMIOKANDE collaboration, K. Bays et al., *Supernova Relic Neutrino Search at Super-Kamiokande*, *Phys. Rev. D* **85** (2012) 052007, [[1111.5031](#)].
- [84] G. J. Feldman and R. D. Cousins, *A Unified approach to the classical statistical analysis of small signals*, *Phys. Rev. D* **57** (1998) 3873–3889, [[physics/9711021](#)].
- [85] ANTARES collaboration, A. Albert et al., *First all-flavor neutrino pointlike source search with the ANTARES neutrino telescope*, *Phys. Rev. D* **96** (2017) 082001, [[1706.01857](#)].

- [86] ICECUBE collaboration, M. G. Aartsen et al., *IceCube Search for Dark Matter Annihilation in nearby Galaxies and Galaxy Clusters*, *Phys. Rev. D* **88** (2013) 122001, [[1307.3473](#)].
- [87] ICECUBE collaboration, M. G. Aartsen et al., *Multipole analysis of IceCube data to search for dark matter accumulated in the Galactic halo*, *Eur. Phys. J. C* **75** (2015) 20, [[1406.6868](#)].
- [88] ICECUBE collaboration, M. G. Aartsen et al., *Search for Dark Matter Annihilation in the Galactic Center with IceCube-79*, *Eur. Phys. J. C* **75** (2015) 492, [[1505.07259](#)].
- [89] A. M. Galper, *The space-based gamma-ray telescope gamma-400 and its scientific goals*, 2013. 10.48550/ARXIV.1306.6175.
- [90] P. Cumani et al., *The GAMMA-400 Space Mission*, in *5th International Fermi Symposium*, 2, 2015, [1502.02976](#).
- [91] K. Engel et al., *The Future of Gamma-Ray Experiments in the MeV-EeV Range*, in *2022 Snowmass Summer Study*, 3, 2022, [2203.07360](#).
- [92] M. Pierre, J. M. Siegal-Gaskins and P. Scott, *Sensitivity of CTA to dark matter signals from the Galactic Center*, *JCAP* **06** (2014) 024, [[1401.7330](#)].
- [93] H. Silverwood, C. Weniger, P. Scott and G. Bertone, *A realistic assessment of the CTA sensitivity to dark matter annihilation*, *JCAP* **03** (2015) 055, [[1408.4131](#)].
- [94] DAMPE collaboration, J. Chang et al., *The DArk Matter Particle Explorer mission*, *Astropart. Phys.* **95** (2017) 6–24, [[1706.08453](#)].
- [95] LHAASO collaboration, G. Di Sciascio, *The LHAASO experiment: from Gamma-Ray Astronomy to Cosmic Rays*, *Nucl. Part. Phys. Proc.* **279–281** (2016) 166–173, [[1602.07600](#)].
- [96] A. Kar, S. Mitra, B. Mukhopadhyaya and T. R. Choudhury, *Can square kilometre array phase 1 go much beyond the lhc in supersymmetry search?*, *Phys. Rev. D* **99** (Jan, 2019) 021302(R).
- [97] A. Kar, S. Mitra, B. Mukhopadhyaya and T. R. Choudhury, *Heavy dark matter particle annihilation in dwarf spheroidal galaxies: radio signals at the SKA telescope*, *Phys. Rev. D* **101** (2020) 023015, [[1905.11426](#)].
- [98] ICECUBE collaboration, M. G. Aartsen et al., *Neutrino astronomy with the next generation IceCube Neutrino Observatory*, [1911.02561](#).
- [99] ICECUBE collaboration, S. Baur, *Dark matter searches with the IceCube Upgrade*, *PoS ICRC2019* (2020) 506, [[1908.08236](#)].
- [100] KM3NET collaboration, D. Lopez-Coto, S. Navas and J. D. Zornoza, *Indirect Dark Matter Searches with the ANTARES and KM3NeT Neutrino Telescopes*, *PoS EPS-HEP2021* (2022) 174.
- [101] KM3NET collaboration, S. Adrian-Martinez et al., *Letter of intent for KM3NeT 2.0*, *J. Phys. G* **43** (2016) 084001, [[1601.07459](#)].
- [102] KM3NET, ANTARES collaboration, P. Fermani, *Status and results from the ANTARES and KM3NeT-ARCA neutrino telescopes*, *PoS NuFact2019* (2020) 032.
- [103] D. López-Coto, *Dark Matter and Solar Atmospheric Neutrino Searches with the KM3NeT-ORCA and ANTARES Neutrino Telescopes*, Ph.D. thesis, Universidad de Granada, Granada U., 2022.
- [104] HYPER-KAMIOKANDE collaboration, K. Abe et al., *Hyper-Kamiokande Design Report*, [1805.04163](#).
- [105] N. F. Bell, M. J. Dolan and S. Robles, *Searching for Sub-GeV Dark Matter in the Galactic Centre using Hyper-Kamiokande*, *JCAP* **09** (2020) 019, [[2005.01950](#)].
- [106] S. Robles, *Disentangling Sub-GeV Dark Matter from the Diffuse Supernova Neutrino Background using Hyper-Kamiokande*, 12, 2022, [2212.07989](#).

- [107] DUNE collaboration, B. Abi et al., *The DUNE Far Detector Interim Design Report Volume 1: Physics, Technology and Strategies*, [1807.10334](#).
- [108] DUNE collaboration, B. Abi et al., *The DUNE Far Detector Interim Design Report, Volume 2: Single-Phase Module*, [1807.10327](#).
- [109] DUNE collaboration, B. Abi et al., *The DUNE Far Detector Interim Design Report, Volume 3: Dual-Phase Module*, [1807.10340](#).
- [110] L. S. Miranda, S. Basegmez du Pree, K. C. Y. Ng, A. Cheek and C. Arina, *Towards detecting super-GeV dark matter via annihilation to neutrinos*, [2211.12235](#).
- [111] K. Akita, G. Lambiase, M. Niibo and M. Yamaguchi, *Neutrino lines from MeV dark matter annihilation and decay in JUNO*, *JCAP* **10** (2022) 097, [[2206.06755](#)].
- [112] C. A. Argüelles et al., *New opportunities at the next-generation neutrino experiments I: BSM neutrino physics and dark matter*, *Rept. Prog. Phys.* **83** (2020) 124201, [[1907.08311](#)].
- [113] GAIA collaboration, A. G. A. Brown et al., *Gaia Data Release 1: Summary of the astrometric, photometric, and survey properties*, *Astron. Astrophys.* **595** (2016) A2, [[1609.04172](#)].
- [114] GAIA collaboration, A. G. A. Brown et al., *Gaia Data Release 2: Summary of the contents and survey properties*, *Astron. Astrophys.* **616** (2018) A1, [[1804.09365](#)].
- [115] M. Pospelov, A. Ritz and M. B. Voloshin, *Secluded WIMP Dark Matter*, *Phys. Lett. B* **662** (2008) 53–61, [[0711.4866](#)].
- [116] A. Berlin, D. Hooper and G. Krnjaic, *Thermal Dark Matter From A Highly Decoupled Sector*, *Phys. Rev. D* **94** (2016) 095019, [[1609.02555](#)].
- [117] J. A. Evans, S. Gori and J. Shelton, *Looking for the WIMP Next Door*, *JHEP* **02** (2018) 100, [[1712.03974](#)].
- [118] D. Hooper, R. K. Leane, Y.-D. Tsai, S. Wegsman and S. J. Witte, *A systematic study of hidden sector dark matter: application to the gamma-ray and antiproton excesses*, *JHEP* **07** (2020) 163, [[1912.08821](#)].
- [119] A. Ibarra, S. Lopez Gehler and M. Pato, *Dark matter constraints from box-shaped gamma-ray features*, *JCAP* **07** (2012) 043, [[1205.0007](#)].
- [120] G. Elor, N. L. Rodd and T. R. Slatyer, *Multistep cascade annihilations of dark matter and the Galactic Center excess*, *Phys. Rev. D* **91** (2015) 103531, [[1503.01773](#)].
- [121] G. Elor, N. L. Rodd, T. R. Slatyer and W. Xue, *Model-Independent Indirect Detection Constraints on Hidden Sector Dark Matter*, *JCAP* **06** (2016) 024, [[1511.08787](#)].
- [122] M. Boudaud, T. Lacroix, M. Stref and J. Lavalle, *Robust cosmic-ray constraints on p-wave annihilating mev dark matter*, *Phys. Rev. D* **99** (Mar, 2019) 061302(R).
- [123] L. Lopez-Honorez, T. Schwetz and J. Zupan, *Higgs portal, fermionic dark matter, and a Standard Model like Higgs at 125 GeV*, *Phys. Lett. B* **716** (2012) 179–185, [[1203.2064](#)].
- [124] G. Arcadi, A. Djouadi and M. Raidal, *Dark Matter through the Higgs portal*, *Phys. Rept.* **842** (2020) 1–180, [[1903.03616](#)].
- [125] G. Arcadi, A. Djouadi and M. Kado, *The Higgs-portal for dark matter: effective field theories versus concrete realizations*, *Eur. Phys. J. C* **81** (2021) 653, [[2101.02507](#)].